Melting of the Chhota Shigri Glacier, Western Himalaya, Insensitive to Anthropogenic Emission Residues: Insights from Geochemical Evidence

S. Nizam[1], I. S. Sen[1], T. Shukla[1] and D. Selby[2, 3]

[1]Department of Earth Sciences, Indian Institute of Technology Kanpur, Kanpur, UP 208016, India.

[2]Department of Earth Sciences, University of Durham, Durham DH1 3LE, UK.

[3]State Key Laboratory of Geological Processes and Mineral Resources, School of Earth.

Corresponding author: S. Nizam (sarwa@iitk.ac.in)

Key Points:

- This study presents first osmium isotopic composition on glacier surface impurities from the Himalaya
- Osmium isotopes and trace metal composition showed predominantly crustal sourced input
- Anthropogenic emission residues are not one of the significant drivers of glacier melting in the western Himalaya, as observed elsewhere.

Abstract

Himalaya glaciers are invariably covered by supra-glacial debris. Of the glaciers the Chhota Shigri Glacier (CSG) in the western Himalaya is basically debris free yet has the highest melt rate compared to other central and eastern Himalayan glaciers. Here, utilizing osmium isotopic composition and major and trace element geochemistry of cryoconite — a dark colored aggregate of mineral and organic materials —and glacial surface materials on the ablation zone of the CSG, we show that the surface of CSG is essentially free of anthropogenically emitted particles, contrary to many previous findings. Given this and the lack of debris, we conclude that the high melting rate in CSG is primarily related to the increase of the Earth's near-surface temperature in direct response to global warming. Thus, monitoring the ice mass loss is further critical given the water source to millions of people.

Plain Language Summary

Industry derived particles are common to Himalayan glaciers being proposed as a major driver to glacier melting. Yet, the abundance of such material is highly variable across the Himalayan. The CSG is a glacier with minimal ice cover yet has a very high ice volume loss. We show that the elevated glacial mass wastage in western Himalaya is insensitive to anthropogenically sourced pollutants but primarily climate controlled.

1 Introduction

Air pollutants of the southern slopes of the Himalayas has reached high-altitude sparsely populated regions such as Khumbu (5079 m a.s.l.) in Nepal (Bonasoni et al., 2010) and Hanle (4520 m a.s.l.) in India (Babu et al., 2011). The pollutants emitted from different anthropogenic sectors in the Indo-Gangetic Plains (Saikawa et al., 2019) are transported to the high-altitude Himalaya by the southwest Indian Summer Monsoon (Cristofanelli et al., 2014; Singh et al., 2020). The presence of anthropogenic emission residues on the Himalayan glaciers has been linked to enhance glacier melting. As a consequence, the ambient air and its suspended particulate matter in high-altitude Himalayan sites have been intensely monitored over last few decades for greenhouse gases and aerosols (Ran et al., 2014; Rupakheti et al., 2017; Shrestha et al., 2010; Stockwell et al., 2016).

Among the particulate impurities, various types of carbon such as organic carbon: (OC), black carbon: (BC), trace metal and biogenic pollutants are the major focus of current research

(Beaudon et al., 2017; Gabrielli et al., 2020; Hong et al., 2009; Kaspari et al., 2011; Nizam et al., 2020; Yan et al., 2019). Studies have shown that the Himalayan ice record exhibits a factor of three increase in BC between 1975-2000 (Kaspari et al., 2011). Similarly, increased anthropogenic metal pollution in glaciers has also been reported in several parts of the central Himalaya and Tibetan Plateau (Beaudon et al., 2017; Gabrielli et al., 2020; Hong et al., 2009; Q. Zhang et al., 2009). Despite the rise in BC concentrations and anthropogenic metal pollution, the concentration of inorganic impurities in the Western Himalayan glaciers remains poorly known.

Existing data in the Western Himalayan region mainly focuses on the source of pollutants (CO_x, NO_x, SO_2, BC, and $PM_{2.5}$) that are mostly derived from receptor and chemical transport modeling, and emission inventories (Alvarado et al., 2018; Bonasoni et al., 2010; Rupakheti et al., 2018; Yarragunta et al., 2020). Although these models provide invaluable insights to the influence of anthropogenic emissions on the western Himalayan cryosphere, the results exhibit disagreement due to the large uncertainties in emission inventories and meteorological parameters. Therefore, given that the Himalayas is neighbored by some of the world's largest emitters of anthropogenic particles, understanding the concentrations, origin, and pathways of other anthropogenically emitted particles, such as metals, is required to ultimately understand the driving mechanism(s) enhancing ice mass wastage and its impact on the downstream population. Understanding the emission source of metals that also emits CO_x, NO_x, SO_2, BC, and $PM_{2.5}$, will permit the independent evaluation of emission sources and support estimates studies based on transport and receptor models (Jeong et al., 2016; Yang et al., 2020).

Thus, to establish the contribution of emission sources to the western Himalayan glaciers, we utilize major and trace element geochemistry together with osmium (Os)— primarily emitted from automobile exhaust catalysts (Poirier & Gariépy, 2005)—isotope systematics of glacial surface impurities. The Os-isotope composition ($^{187}Os/^{188}Os$) of natural and anthropogenic materials only records the time-integrated fractionation of the Re/Os ratio in the sources. Due to the extremely long half-life of ^{187}Re (ca. 42 billion years), the present-day $^{187}Os/^{188}Os$ composition of natural and anthropogenic materials practically remains constant throughout the process of particle generation, transportation, and deposition. As a result, the Re-Os isotopic system is an emerging tool widely used in tracing anthropogenic sources in precipitation, snow, and ice in remote regions (Chen et al., 2009; Rauch et al., 2005; Rodushkin et al., 2007; Sen et al., 2013), as

well as marine systems (Ownsworth et al., 2019; Sproson et al., 2020). As such, the objective of the study is to apply major and trace element geochemistry, coupled with $^{187}Os/^{188}Os$ compositions of cryoconite and moraine samples to constrain the metal composition across the ablation zone of the Chhota Shigri Glacier (CSG) in the western Himalaya. The latter is used to evaluate and discuss the sources of the metal impurities on the ablation zone of CSG in relation to the reported values for the Himalayan glaciers and ultimately the relationships to the driving mechanisms of glacier mass wasting.

2 Materials and Methods

2.1 Sample Collection

Twenty samples of supraglacial cryoconite were collected from cryoconite holes across the entire ablation zone of the CSG between 4500 to 4930 m a.s.l. (details in Text S1-S2 and Figure S1). The light grey to dark black colored sediments was collected into Corning® 50 mL centrifuge tube using pre-cleaned plastic scoops. In addition to the cryoconite samples, seven moraine debris samples of ca. 0.3-0.5 kg (cobbles to clay size) were also collected in polyethylene sterile Whirl-Pack® bags. All samples were kept frozen prior to analysis. To permit evaluation of anthropogenic emission particulates in the CSG our sample set also comprises samples of Gondwana and Tertiary coal from two major coalfields of India (Jharia in the state of Jharkhand and Makum in the state of Assam), and diesel engine exhaust particulates obtained from engine-exhaust experiments (Text S3).

2.2 Rhenium-Osmium (Re-Os) Analysis

Cryoconite and moraine samples were dried, sieved (moraine only) and powdered for geochemical analysis (details in Text S4). Ten cryoconite, two moraine samples (<63 µm fraction), four coal samples, and two engine exhaust particulates samples were selected for Re-Os analysis. The Re-Os concentration and isotopic compositions were determined at the Durham Geochemistry Centre using aqua regia carius-tube digestion isotope-dilution negative ion mass spectrometry analytical protocols (Cumming et al., 2013; Selby et al., 2009). Approximately, 1 g of cryoconite and moraine, 0.2 g of coal, and 0.02 to 0.03 g of exhaust particulate were loaded into a carius tube with a known amount of mixed tracer solution (spike) of ^{190}Os and ^{185}Re and 9 ml of aqua regia solution. The carius tube was sealed and heated to 240 °C for 48 hours. The Os of the digested samples was isolated and purified using standard solvent extraction ($CHCl_3$) and micro-distillation

(CrO_3-H_2SO_4-HBr). The Re fraction was isolated and purified using NaOH-acetone solvent extraction and anion chromatography. The isolated Re and Os fractions were loaded onto Ni and Pt filament, respectively. The Re and Os isotopic compositions were determined using negative thermal ionization mass spectrometry using a Thermo Fisher TRITON mass spectrometer via static Faraday collection mode for Re and ion-counting using a secondary electron multiplier in the peak-hopping mode for Os. Total procedural blanks were 2.1± 0.02 and 0.1± 0.01 ppt for Re and Os, respectively, with an average $^{187}Os/^{188}Os$ value of 0.25± 0.03 (n = 2) for cryoconite and moraine analysis, and 2.3± 0.2 and 0.1± 0.02 ppt for Re and Os, respectively, with an average $^{187}Os/^{188}Os$ value of 0.20± 0.06 (n = 4) for coal and exhaust particulate analysis. In-house standard solution measurements yielded $^{185}Re/^{187}Re$ value of 0.59786± 0.00014 (1 SD, n = 7) for the Re solution and a $^{187}Os/^{188}Os$ value of 0.16085± 0.00017 (1 SD, n = 6) for the Durham Romil Osmium Solution (DROsS), which are in agreement with those reported in the previous studies (Percival et al., 2019). The average value plus uncertainty of the Re standard solution together with the natural $^{185}Re/^{187}Re$ value of 0.5974 (Gramlich et al., 1973) is used for the Re sample mass fractionation correction. Data reduction includes the instrumental mass fractionation, isobaric oxygen interference, and contribution of blanks and the tracer solution. The final two-sigma uncertainties of the Re-Os data include the fully propagated uncertainties of sample-spike weighing, tracer calibration, blank abundances, and isotope compositions, and the intermediate precision of the repeated measurements on the Re and Os reference solutions.

3 Results

3.1 Trace Element Systematics

Trace element concentrations of the cryoconite, bulk, and fine moraine normalized to the local rock composition is shown in Figure S2. The fine moraine fractions and cryoconite exhibit similar patterns but possess higher trace element concentrations in comparison to the bulk moraine fractions that resemble local rock compositions. The higher trace element concentrations in the fine moraine compared to bulk fraction are consistent with additional contamination/mixing or grain size/mineral sorting related enrichment as heavy metals (except Pb) including Sc, Ga, Sr, Nb, and Ta negatively correlate with SiO_2 (Pearson correlation coefficients $R \geq -0.70$ to -0.94, p =0.001-0.05; Figure S3a and S4) (Cai et al., 2015; Thorpe et al., 2019). Additionally, an overall negative correlation is exhibited between other elements (except Li, Be, Rb, Cs, Ta and Ba) against

SiO_2. A similar relationship is exhibited between trace metals and SiO_2 in cryoconite samples (Figure S3b). In comparison to the fine moraine fraction, the cryoconite samples exhibit higher concentrations of V, Cr, Co, Ni, and Cd in more than 50% of the samples. Chondrite normalized REE concentrations show LREE enrichment and a negative Eu anomaly for cryoconites and all moraine fractions (Figure S5).

The relationship of the cryoconite trace element ratios to the local rock composition suggests that the cryoconite composition has a local crustal provenance. For example, Cd/Zn (0.001-0.007) and Pb/Cu (0.84-1.98) ratios are similar to that of the local rock signature (Cd/Zn = 0.001-0.014 and Pb/Cu = 0.45-5.87). Further, REE ratios including, La/Ce, La/Sm, La/Yb and La/Lu ratios of cryoconite that vary between 0.44-0.51, 30-57, 15-26, and 106-194, respectively, are similar to local rock values (0.37-0.48, 33-91, 15-41 and 113-317, respectively). Noteworthy, the La/Ce, La/Sm, La/Yb and La/Lu ratios of cryoconite and moraine are much lower than anthropogenic emission sources (La/Ce = 1.3-1.8, La/Sm = 19-28, La/Yb = 135-950, La/Lu = 5400-1000) (Kitto et al., 1992; Olmez & Gordon, 1985). As are the Co/Cs ratios in the cryoconite samples (0.25 and 2.85, average = 1.12± 0.78,. versus >2.5 for anthropogenic emissions (Geagea et al., 2007). Further, with the exception of Cr, Ni, and Cd, the enrichment factors (EF) values of ≤1 support a predominant crustal provenance for the cryoconite (Figure S6). The EF values for Cr (2.2), Ni (2.7) and Cd (2.6) in cryoconite show a detectable non-crustal input.

3.2 Re-Os Systematics

Rhenium and Os concentrations of the cryoconite, moraine, coal, and vehicular exhaust samples are reported in Table 1. In Figure 1a, the Re (ppb) and Os (ppt) concentrations together with TOC (%) are shown for cryoconite and the fine moraine fraction. Overall, cryoconite sampled between 4700-4930 m a.s.l. possess higher average TOC (~1.7 %), Re (0.24-0.47 ppb), and Os (37-104 ppt) in comparison to cryoconite sampled between 4500-4700 m a.s.l. (average TOC = 0.8 %; Re = 0.16-0.21 ppb; Os = 11-32 ppt). The elevated TOC, Re and Os concentrations in cryoconite above 4700 m a.s.l. also correspond to higher concentration of heavy metals (Figure 1b). For example, trace metals such as Cr, V, Co, Cu, and Zn follow the trends shown by Re and Os suggesting that these elements are probably controlled by common mineral/sources (Chen et al., 2016). The absolute abundances of Re and Os show a moderate positive correlation (R= 0.58, p = 0.1) (Figure S3b and S7), with a similar correlation exhibited with TOC (R= 0.71 and 0.53,

respectively). The cryoconite $^{187}Os/^{188}Os$ composition fall between 0.38 and 1.31, with cryoconite between 4700-4930 m a.s.l. possessing $^{187}Os/^{188}Os$ values between 0.38 and 0.83. Below 4700 m a.s.l. the cryoconite samples possess more radiogenic $^{187}Os/^{188}Os$ values. The $^{187}Os/^{188}Os$ ratios show a significant negative correlation with Os concentrations (R= -0.94, p = 0.001; Figure S3b and S7). Further, the $^{187}Os/^{188}Os$ ratios correlate positively with major oxides such as SiO_2, Na_2O, and K_2O (R = 0.71-0.89, p = 0.001-0.05). In contrast, heavy REE (HREE: Er to Lu), MgO, Fe_2O_3, MnO, and TiO_2 exhibit a significant negative correlation with $^{187}Os/^{188}Os$ ratios (R= -0.81 to -0.93, p =0.001-0.01; Figure S7 and S8).

The Re and Os concentrations of two moraine samples from ~4750 and 4550 m a.s.l are 0.14 and 0.21 ppb and 13 and 30 ppt, being similar to the average upper continental crust (UCC) composition (Re = ~0.20 ppb; Os = ~31 ppt) (Esser & Turekian, 1993; Peucker-Ehrenbrink & Jahn, 2001). The Re and Os concentrations in Gondwana coal range between 0.26 and 0.76 ppb and 7 and 18 ppt, respectively. For the Tertiary coal samples, the Re and Os concentrations range between 0.47 and 0.53 ppb and 63 and 726 ppt, respectively. Unlike cryoconite, the Gondwana and Tertiary coal show limited variability and are characterized by radiogenic ($^{187}Os/^{188}Os$ =1.61-1.64) and unradiogenic osmium isotope compositions ($^{187}Os/^{188}Os$ = 0.14 and 0.21), respectively. The analysis of two engine exhausts yielded Re and Os concentrations of 0.07 and 1.04 ppb and 2 and 6 ppt, respectively. The engine exhaust samples are characterized by an unradiogenic osmium isotope composition ($^{187}Os/^{188}Os$ = 0.21-0.22), similar to catalytic converters (Poirier & Gariépy, 2005).

4 Discussion

4.1 Cryoconite Provenance

Glaciers are sites of active physical erosion, with their continuous movement effectively powdering rock units in the glacial catchment that can be further eroded by wind action and deflation (Brown et al., 1996; Sharp et al., 1995; Tranter et al., 2002). This local freshly weathered rock that is subjected to deflation will overwhelm any long-range dust transport signal by covering the neighboring glacier. This is illustrated by both the major (Figure S9) and trace element systematics (Figure S2) of the CSG cryoconite, which are derived from weakly weathered rocks of the glacial catchment. Most of the cryoconite (14 samples,) exhibit Co, Cr, Ni and Sc enrichment that indicate a detectable non-crustal component. In contrast, cryoconite from Arctic, European,

Canadian and other South Asian glaciers exhibit several orders of magnitude higher heavy metal enrichment compared to its local rock and moraine and were consistent with high activity concentrations of anthropogenic radionuclides. (Baccolo et al., 2017; Beaudon et al., 2017; Łokas et al., 2016; Owens et al., 2019; Singh et al., 2013). This suggests that the CSG seems relatively pristine compared to other glaciers where significant anthropogenic pollution signal has been recorded due to long range transport of the anthropogenic emission residues. Moreover, samples showing detectable metal enrichment in the CSG ablation occur mainly in the upper reaches (except first sample) of the glacier ablation zone i.e. above 4700 m a.s.l. These samples further show minor deviation from the local moraine composition towards a more mafic rock composition (Figure S10 and S11). Although heavy metals enrichment can also be attributed to anthropogenic contributions, but correlation with TOC suggest that the enrichment seems most plausibly attributed to sources of TOC (microorganisms) owing to its inherent characteristics to accumulate fine particulates (Łokas et al., 2016). Furthermore, given that air-mass back trajectory modeling clearly shows that 50% of the air mass that reaches the glaciers originates from the west, within ~250 km of the study site, and possesses limited inputs from the Indo-Gangetic Basin (Nizam et al., 2020), only minor input from anthropogenic sources can be considered. Lastly, the chondrite normalized REE signature of moraine, local country rocks from the Himalaya, river sediments from glacial catchments, cryoconite, snow and ice core dust (Figure S12) show similar REE patterns, all exhibiting REE enrichment, similar to granitic or shale (PAAS)-like sources, which are commonly observed in the Higher and the Lesser Himalayan rocks and sediment. The anthropogenic dust mostly exhibits fractionated (enriched) LREE patterns with smooth HREE enrichment, and often contains a strong positive Gd anomaly (Geagea et al., 2007; Hatje et al., 2016). The cryoconite show a large range in $^{187}Os/^{188}Os$ compositions that overlap with both natural and anthropogenic sources that do not exhibit singular $^{187}Os/^{188}Os$ signatures (Figure 2).

The cryoconite unradiogenic $^{187}Os/^{188}Os$ signature can be explained by both contributions from natural Os sources such as cosmic dust, volcanic aerosols, mafic and ultramafic rocks, as well as anthropogenic Os from catalytic converters that are often recycled ($^{187}Os/^{188}Os$ = ~0.38) (Poirier & Gariépy, 2005), fossil fuels, smelting of chromite, base-metal sulfide, and PGE ores and municipal solid waste incinerators (MSWIs). Contributions from volcanic aerosols and cosmic dust seem unlikely due to the absence of active volcanism in and around the Himalaya (Fitch, 1970), and the extremely low (40,000± 20,000 t yr^{-1}; t=10^6 g) global cosmic dust flux (Love &

Brownlee, 1993) that can significantly affect the $^{187}Os/^{188}Os$ of sediments in the highly active glacial ablation zones. Contribution from mafic rocks is plausible as ultramafic dykes, sills, and pegmatitic veins (early Proterozoic-late Paleozoic age) are common in HHCS and locally in the glacial catchment (Thakur & Patel, 2012; Thöni et al., 2012). Given that the unradiogenic $^{187}Os/^{188}Os$ signature in the cryoconite correlates with high Fe_2O_3-MgO and low SiO_2 concentrations (Figure S8), a mafic/ultramafic source rock input is likely as supported by the cryoconite trace element geochemistry. Therefore, from trace element systematics, Re and Os concentrations, and $^{187}Os/^{188}Os$ compositions it can be concluded that the glacial debris contains felsic and mafic/ultramafic rock components, with essentially no input from anthropogenic sources.

4.2 Further Evaluation of Natural and Anthropogenic Sourced Osmium

The relative contributions from various source end-members are quantified using a three-component mixing model using $^{187}Os/^{188}Os$ and Os concentration as tracers. The first end-member represents local rocks, which is very similar in composition to the Higher Himalayan Crystalline Sequence (Pierson-Wickmann et al., 2000) and eroding UCC (Peucker-Ehrenbrink & Jahn, 2001). For which, we assign an Os abundance of 30.4 ppt and $^{187}Os/^{188}Os$ value of ~1.48 (Table 1). For the second end-member, mafic-ultramafic rocks are selected having an Os concentration of 850 ppt and an $^{187}Os/^{188}Os$ value of ~0.12 (Table 4; Data from (Meisel et al., 2001), Sample Number: KH80-100, peridotite xenoliths). To explain the data distribution (Figure 3a), the third end-member should contain low Os concentration and an intermediate $^{187}Os/^{188}Os$ composition. This end-member could represent an Os-poor mineral such as aeolian quartz or granitoid and/or gneisses (Peucker-Ehrenbrink & Blum, 1998) and therefore we assign an Os concentration of 1 ppt and a $^{187}Os/^{188}Os$ value of ~0.90. It is noteworthy that the $^{187}Os/^{188}Os$ composition could be more radiogenic and Os concentrations can be significantly lower (Peucker-Ehrenbrink & Blum, 1998). Keeping in mind that the three end-members of our mixing model should enclose all data points (Figure 3a), we performed our mixing model with the defined end-members as outlined above. Our mixing calculations suggest that the cryoconite $^{187}Os/^{188}Os$ signature is derived from local rocks (67.4± 18.6%), with fractional contributions from an Os-poor mineral phase (29.6± 19.9%), and limited input from the mafic-ultramafic rocks (3.0± 2.8%, Table S4, Figure 3b). In

general, the upper elevation of the glacier showed a greater Os contribution from mafic rock/mineral phase, which is consistent with the trace element systematics (Figure 1b).

We acknowledge that the choice of end-member compositions will change the end-member contributions, but we emphasize that the conclusion of the study will not change. Further, we did not include any anthropogenic sources because enrichment factors, trace and major elements, supports a predominant crustal provenance for the cryoconite. Moreover, this is supported by the fact that the glacier ablation zone is free of fossil fuel derived carbon (Nizam et al., 2020) and therefore we did not include coal and engine exhaust as suitable end-members. We additionally emphasize that the metal enrichment in the cryoconites can also be modified (enriched) by microbial processes. Given the elevated TOC concentration observed in upper ablation zone of the CSG a higher level of microbial activity is implied (Anesio et al., 2009). The $\delta^{13}C$ enrichment (-18.19‰) in cryoconite samples and its relationship with N enrichment and or depletion supports contributions from photo-autotrophic and heterotrophic micro-organisms that may have also modified predominantly heavy metal (Cr, V, Ni, and Co) signature (Nizam et al., 2020).

4.3 Implications of Absence of Anthropogenic Emission Residues in the Western Himalayan Glacier

The Himalayan glaciers receive a large supply of metals in the form of mineral dust from wind-blown rock dust from the erosion of the UCC and mafic rocks, with inputs from anthropogenic sources (Casey, 2012; Cristofanelli et al., 2014; Wake et al., 1993). The knowledge of the amount, composition, and source of dust and anthropogenic emission is essential to calculate the heat-absorbing capacity of the residue, and in turn, ice melting rates. For example, 1 ppb of BC residue on the glacier has the same effect on albedo as that of 75 ppb dust (Jacobi et al., 2015). In this study, we show that CSG has negligible metal impurity residues from anthropogenic sources. Further, carbon characterization (Ramped Pyrolysis Oxidation, RPO, $\delta^{13}C$**,** and ^{14}C chronology) of total organic carbon (OC) in both cryoconite and the <63 µm fraction of moraine from the same glacier reveals that the cryoconite have negligible contributions from fossil fuel emission sources (Nizam et al., 2020). The RPO, $\delta^{13}C$, and ^{14}C data reveal that 98.3± 1.6% of the OC is sourced from local biomass sources, atmospheric organic matter, and glacial microbes, with only 1.7± 1.6% of the OC being sourced from petrogenetic sources. Further, previously we have shown that the 50% of the air mass (annual basis) originates far (>1000 km) from west of the

receptor (CSG) site (Nizam et al., 2020). Therefore, based on the Os isotopic systematics and previous findings we conclude that the CSG is essentially free of anthropogenic residues and receives limited long-range dust inputs.

It is well established that glaciers in the CSG basin are losing mass at an average rate of 0.50 meter water-equivalent per year (m w.e. yr^{-1}) over the last two decades (Azam et al., 2019), which is higher than the central (0.35 m w.e. yr^{-1}) and eastern Himalayan (0.43 m w.e. yr^{-1}) glaciers having higher debris covered glaciers (18-24%) and substantial contribution of anthropogenic sourced pollutants from the Indian subcontinent (Babu et al., 2011; Brun et al., 2017; Li et al., 2016). The high glacial mass wastage rate observed in western Himalaya is likely due to elevated mean annual tropospheric warming trend (0.016 ± 0.005 ^{o} K/year) during ablation season, which is higher than Central and Eastern Himalayan region (Prasad et al., 2009). Consequently, warming induced melting of snow (which is 80% of total precipitation) constitute the largest faction (15-66%) of the annual hydrological budget in the western Himalaya (Azam et al., 2019; Bookhagen & Burbank, 2010). In contrast, central and western Himalayan glaciers are Indian Summer Monsoon fed (contribute ~80% of the annual hydrological budget) and receives significant fraction of anthropogenic (50% of total anthropogenic carbon) pollutants from the heavily polluted Indo-Gangetic Plains (Li et al., 2016) that can pose an additional melting stress of 340 kg m^{-2} yr^{-1} (Ginot et al., 2014).

The near absence of anthropogenic particles on the nearly debris free CSG therefore reveals that heat-absorbing anthropogenic particles deposited on the surface of the CSG are not one of the primary drivers behind CSG melting, as observed in other parts of the world such as the Greenland, Alaska, and Tibet (Dumont et al., 2014; Nagorski et al., 2019; Xu et al., 2009). Despite an increase in anthropogenic emissions in the Indian subcontinent over the last 50 years (Crippa et al., 2018), we conclude that anthropogenic emission residues on the surface of CSG will not significantly enhance the glacier mass wastage rates in CSG in the near future. The rapid retreat of CSG can be best explained by elevated temperature trends and morphological characteristic of the catchment (Gantayat et al., 2017). It is noteworthy that numerical modeling of CSG reveals that the glacier will cease to exist by AD 2109 with a temperature rise of 5.5 K. (Gantayat et al., 2017).

5 Conclusions

The concentration, origin, and pathways of metals over the CSG was investigated for the first time using major and trace elements, and Re-Os isotope systematics of supraglacial debris namely from cryoconite and moraine samples. Our study highlights two important points regarding the presence of metal impurities on the CSG glacier surface. Firstly, although the Himalaya is surrounded by some of the world's largest emitter of anthropogenic particles, we find limited anthropogenic metal impurities over the CSG likely due to the source region of the air mass reaching the CSG. Mixing model calculations show that Os in the CSG is exclusively sourced from crustal rocks. Secondly, integration of geochemical and air-mass back trajectory modeling data reveal that the sediment/dust is mostly of local origin. We conclude that the enhanced CSG melting rate is insensitive to organic and inorganic anthropogenic emission deposits on the surface of the CSG glacier, and predominately controlled by climate warming.

Data availability

Full data and supporting information are available as supplementary material. We assure that the supplementary will be made available in suitable data repository archive upon acceptance of the manuscript.

Author contributions

I.S.S. conceived the study. S.N. performed laboratory measurements. S.N., I.S.S., T.S. and D.S. analysed the data. S.N. and I.S.S. wrote the paper with input from all authors. I.S.S. handled funding acquisition.

Competing interests

The authors declare that they have no competing interests.

Acknowledgements

This project is financially supported by Department of Science and Technology, Government of India, Climate Change Program (SPLICE) Grant DST/CCP/Aerosol/86/2017(C) and Science & Engineering Research Board (SERB) Grant (EMR/2015/000439) to I.S. Sen. S. Nizam is thankful to Indian Institute of Technology-Kanpur (IIT-Kanpur) for Ph.D. scholarship. We thank IIT-Kanpur and Durham University for providing access to instrumentation and support. We are thankful to Mohd. Farooq Azam from IIT Indore for field sampling support. Sincere thanks to A.K. Agarwal to provide access to the Engine Research Lab. Discussion with Michal Bizimis, Thomas Meisel, and Soumita Boral greatly acknowledged. DS acknowledges the technical support of Chris Ottley, Geoff Nowell, and Antonia Hofmann, and also the support of the TOTAL Endowment Fund and the Dida Scholarship of CUG.

Supplementary Materials:

Text S1-S5

Figure S1-S12 and their captions.

Table S1-S4 and their captions.

References

van Acken, D., Tütken, T., Daly, J. S., Schmid-Röhl, A., & Orr, P. J. (2019). Rhenium-osmium geochronology of the Toarcian Posidonia Shale, SW Germany. *Palaeogeography, Palaeoclimatology, Palaeoecology*, *534*, 109294. https://doi.org/10.1016/j.palaeo.2019.109294

Ackerman, L., Pašava, J., Šípková, A., Martínková, E., Haluzová, E., Rodovská, Z., & Chrastný, V. (2019). Copper, zinc, chromium and osmium isotopic compositions of the Teplá-Barrandian unit black shales and implications for the composition and oxygenation of the Neoproterozoic-Cambrian ocean. *Chemical Geology*, *521*, 59–75. https://doi.org/10.1016/j.chemgeo.2019.05.013

Agarwal, A. K., Singh, A. P., Gupta, T., Agarwal, R. A., Sharma, N., Rajput, P., et al. (2018). Mutagenicity and Cytotoxicity of Particulate Matter Emitted from Biodiesel-Fueled Engines. *Environmental Science & Technology*, *52*(24), 14496–14507. research-article. https://doi.org/10.1021/acs.est.8b03345

Alvarado, M. J., Winijkul, E., Adams-Selin, R., Hunt, E., Brodowski, C., Lonsdale, C. R., et al. (2018). Sources of Black Carbon Deposition to the Himalayan Glaciers in Current and Future Climates. *Journal of Geophysical Research: Atmospheres*, *123*(14), 7482–7505. https://doi.org/10.1029/2018JD029049

Anesio, A. M., Hodson, A. J., Fritz, A., Psenner, R., & Sattler, B. (2009). High microbial activity on glaciers: importance to the global carbon cycle. *Global Change Biology*, *15*(4), 955–960. https://doi.org/10.1111/j.1365-2486.2008.01758.x

Azam, M. F., Wagnon, P., Vincent, C., Ramanathan, A., Favier, V., Mandal, A., & Pottakkal, J. G. (2014). Processes governing the mass balance of Chhota Shigri Glacier (western Himalaya, India) assessed by point-scale surface energy balance measurements. *The Cryosphere*, *8*(6), 2195–2217. https://doi.org/10.5194/tc-8-2195-2014

Azam, Mohd Farooq, Wagnon, P., Vincent, C., Ramanathan, A., Kumar, N., Srivastava, S., et al. (2019). Snow and ice melt contributions in a highly glacierized catchment of Chhota Shigri Glacier (India) over the last five decades. *Journal of Hydrology*, *574*, 760–773. https://doi.org/10.1016/j.jhydrol.2019.04.075

Babu, S. S., Chaubey, J. P., Krishna Moorthy, K., Gogoi, M. M., Kompalli, S. K., Sreekanth, V., et al. (2011). High altitude (~4520 m amsl) measurements of black carbon aerosols over western trans-Himalayas: Seasonal heterogeneity and source apportionment. *Journal of Geophysical Research: Atmospheres*, *116*(D24), n/a-n/a. https://doi.org/10.1029/2011JD016722

Baccolo, G., Di Mauro, B., Massabò, D., Clemenza, M., Nastasi, M., Delmonte, B., et al. (2017). Cryoconite as a temporary sink for anthropogenic species stored in glaciers. *Scientific Reports*, *7*(1), 9623. https://doi.org/10.1038/s41598-017-10220-5

Barbieri, M. (2016). The Importance of Enrichment Factor (EF) and Geoaccumulation Index (Igeo) to Evaluate the Soil Contamination. *Journal of Geology & Geophysics*, *5*(1), 1000237. https://doi.org/10.4172/2381-8719.1000237

Beaudon, E., Gabrielli, P., Sierra-Hernández, M. R., Wegner, A., & Thompson, L. G. (2017). Central Tibetan Plateau atmospheric trace metals contamination: A 500-year record from the Puruogangri ice core. *Science of The Total Environment*, *601–602*, 1349–1363. https://doi.org/10.1016/j.scitotenv.2017.05.195

Bonasoni, P., Laj, P., Marinoni, A., Sprenger, M., Angelini, F., Arduini, J., et al. (2010). Atmospheric Brown Clouds in the Himalayas: first two years of continuous observations at the Nepal Climate Observatory-Pyramid (5079 m). *Atmospheric Chemistry and Physics*, *10*(15), 7515–7531. https://doi.org/10.5194/acp-10-7515-2010

Bookhagen, B., & Burbank, D. W. (2010). Toward a complete Himalayan hydrological budget: Spatiotemporal distribution of snowmelt and rainfall and their impact on river discharge. *Journal of Geophysical Research*, *115*(F3), F03019. https://doi.org/10.1029/2009JF001426

Brown, G. H., Sharp, M., & Tranter, M. (1996). Subglacial chemical erosion: seasonal variations in solute provenance, Haut Glacier D'Arolla, Valais, Switzerland. *Annals of Glaciology*, *22*, 25–31. https://doi.org/10.3189/1996AoG22-1-25-31

Brun, F., Wagnon, P., Berthier, E., Jomelli, V., Maharjan, S. B., Shrestha, F., & Kraaijenbrink, P. D. A. (2019). Heterogeneous Influence of Glacier Morphology on the Mass Balance Variability in High Mountain Asia. *Journal of Geophysical Research: Earth Surface*, *124*(6), 1331–1345. https://doi.org/10.1029/2018JF004838

Brun, Fanny, Berthier, E., Wagnon, P., Kääb, A., & Treichler, D. (2017). A spatially resolved estimate of High Mountain Asia glacier mass balances from 2000 to 2016. *Nature Geoscience*, *10*(9), 668–673. https://doi.org/10.1038/ngeo2999

Cai, L., Xu, Z., Bao, P., He, M., Dou, L., Chen, L., et al. (2015). Multivariate and geostatistical analyses of the spatial distribution and source of arsenic and heavy metals in the agricultural soils in Shunde, Southeast China. *Journal of Geochemical Exploration*, *148*, 189–195. https://doi.org/10.1016/j.gexplo.2014.09.010

Casey, K. A. (2012). Supraglacial dust and debris: geochemical compositions from glaciers in Svalbard, southern Norway, Nepal and New Zealand. *Earth System Science Data Discussions*, *5*(1), 107–145. https://doi.org/10.5194/essdd-5-107-2012

Castillo, S., Moreno, T., Querol, X., Alastuey, A., Cuevas, E., Herrmann, L., et al. (2008). Trace element variation in size-fractionated African desert dusts. *Journal of Arid Environments*, *72*(6), 1034–1045. https://doi.org/10.1016/j.jaridenv.2007.12.007

Chang, Q., Mishima, T., Yabuki, S., Takahashi, Y., & Shimizu, H. (2000). Sr and Nd isotope ratios and REE abundances of moraines in the mountain areas surrounding the Taklimakan Desert, NW China. *GEOCHEMICAL JOURNAL*, *34*(6), 407–427. https://doi.org/10.2343/geochemj.34.407

Chen, C., Sedwick, P. N., & Sharma, M. (2009). Anthropogenic osmium in rain and snow reveals global-scale atmospheric contamination. *Proceedings of the National Academy of Sciences*, *106*(19), 7724–7728. https://doi.org/10.1073/pnas.0811803106

Chen, K., Walker, R. J., Rudnick, R. L., Gao, S., Gaschnig, R. M., Puchtel, I. S., et al. (2016). Platinum-group element abundances and Re–Os isotopic systematics of the upper continental crust through time: Evidence from glacial diamictites. *Geochimica et Cosmochimica Acta*, *191*, 1–16. https://doi.org/10.1016/j.gca.2016.07.004

Coggon, J. A., Nowell, G. M., Pearson, D. G., Oberthür, T., Lorand, J.-P., Melcher, F., & Parman, S. W. (2012). The 190Pt–186Os decay system applied to dating platinum-group element mineralization of the Bushveld Complex, South Africa. *Chemical Geology*, *302–303*, 48–60. https://doi.org/10.1016/j.chemgeo.2011.10.015

Cogley, J. G. (2012). Himalayan glaciers in the balance. *Nature*, *488*(7412), 468–469. https://doi.org/10.1038/488468a

Corrick, A. J., Selby, D., McKirdy, D. M., Hall, P. A., Gong, S., Trefry, C., & Ross, A. S. (2019). Remotely constraining the temporal evolution of offshore oil systems. *Scientific Reports*, *9*(1), 1327. https://doi.org/10.1038/s41598-018-37884-x

Crippa, M., Guizzardi, D., Muntean, M., Schaaf, E., Dentener, F., van Aardenne, J. A., et al. (2018). Gridded emissions of air pollutants for the period 1970–2012 within EDGAR v4.3.2. *Earth System Science Data*, *10*(4), 1987–2013. https://doi.org/10.5194/essd-10-1987-2018

Cristofanelli, P., Putero, D., Adhikary, B., Landi, T. C., Marinoni, A., Duchi, R., et al. (2014). Transport of short-lived climate forcers/pollutants (SLCF/P) to the Himalayas during the South Asian summer monsoon onset. *Environmental Research Letters*, *9*(8), 084005. https://doi.org/10.1088/1748-9326/9/8/084005

Cumming, V. M., Poulton, S. W., Rooney, A. D., & Selby, D. (2013). Anoxia in the terrestrial environment during the late Mesoproterozoic. *Geology*, *41*(5), 583–586. https://doi.org/10.1130/G34299.1

Cumming, V. M., Selby, D., Lillis, P. G., & Lewan, M. D. (2014). Re–Os geochronology and Os isotope fingerprinting of petroleum sourced from a Type I lacustrine kerogen: Insights from the natural Green River petroleum system in the Uinta Basin and hydrous pyrolysis experiments. *Geochimica et Cosmochimica Acta*, *138*, 32–56. https://doi.org/10.1016/j.gca.2014.04.016

Das, B. K., & Haake, B.-G. (2003). Geochemistry of Rewalsar Lake sediment, Lesser Himalaya, India: implications for source-area weathering, provenance and tectonic setting. *Geosciences Journal*, *7*(4), 299–312. https://doi.org/10.1007/BF02919560

Dumont, M., Brun, E., Picard, G., Michou, M., Libois, Q., Petit, J.-R., et al. (2014). Contribution of light-absorbing impurities in snow to Greenland's darkening since 2009. *Nature Geoscience*, *7*(7), 509–512. https://doi.org/10.1038/ngeo2180

Esser, B. K., & Turekian, K. K. (1993). The osmium isotopic composition of the continental crust. *Geochimica et Cosmochimica Acta*, *57*(13), 3093–3104. https://doi.org/10.1016/0016-7037(93)90296-9

Ferrat, M., Weiss, D. J., Strekopytov, S., Dong, S., Chen, H., Najorka, J., et al. (2011). Improved provenance tracing of Asian dust sources using rare earth elements and selected trace elements for palaeomonsoon studies on the eastern Tibetan Plateau. *Geochimica et Cosmochimica Acta*, *75*(21), 6374–6399. https://doi.org/10.1016/j.gca.2011.08.025

Fitch, T. J. (1970). Earthquake mechanisms in the Himalayan, Burmese, and Andaman Regions and continental tectonics in central Asia. *Journal of Geophysical Research*, *75*(14), 2699–2709. https://doi.org/10.1029/JB075i014p02699

Funari, V., Meisel, T., & Braga, R. (2016). The potential impact of municipal solid waste incinerators ashes on the anthropogenic osmium budget. *Science of The Total Environment*, *541*, 1549–1555. https://doi.org/10.1016/j.scitotenv.2015.10.014

Gabrielli, P., Wegner, A., Sierra-Hernández, M. R., Beaudon, E., Davis, M., Barker, J. D., & Thompson, L. G. (2020). Early atmospheric contamination on the top of the Himalayas since the onset of the European Industrial Revolution. *Proceedings of the National Academy of Sciences*, *117*(8), 3967–3973. https://doi.org/10.1073/pnas.1910485117

Gantayat, P., Kulkarni, A. V., Srinivasan, J., & Schmeits, M. J. (2017). Numerical modelling of past retreat and future evolution of Chhota Shigri glacier in Western Indian Himalaya. *Annals of Glaciology*, *58*(75pt2), 136–144. https://doi.org/10.1017/aog.2017.21

Geagea, M. L., Stille, P., Millet, M., & Perrone, T. (2007). REE characteristics and Pb, Sr and Nd isotopic compositions of steel plant emissions. *Science of The Total Environment*, *373*(1), 404–419. https://doi.org/10.1016/j.scitotenv.2006.11.011

Ginot, P., Dumont, M., Lim, S., Patris, N., Taupin, J. D., Wagnon, P., et al. (2014). A 10 year record of black carbon and dust from a Mera Peak ice core (Nepal): Variability and potential impact on melting of Himalayan glaciers. *Cryosphere*, *8*(4), 1479–1496. https://doi.org/10.5194/tc-8-1479-2014

Gramlich, J. W., Murphy, T. J., Garner, E. L., & Shields, W. R. (1973). Absolute isotopic abundance ratio

485 and atomic weight of a reference sample of rhenium. *Journal of Research of the National Bureau of*
486 *Standards Section A: Physics and Chemistry*, *77A*(6), 691. https://doi.org/10.6028/jres.077A.040

487 Hanski, E., Walker, R. J., Huhma, H., & Suominen, I. (2001). The Os and Nd isotopic systematics of c.
488 2.44 Ga Akanvaara and Koitelainen mafic layered intrusions in northern Finland. *Precambrian*
489 *Research*, *109*(1–2), 73–102. https://doi.org/10.1016/S0301-9268(01)00142-5

490 Hatje, V., Bruland, K. W., & Flegal, A. R. (2016). Increases in Anthropogenic Gadolinium Anomalies
491 and Rare Earth Element Concentrations in San Francisco Bay over a 20 Year Record.
492 *Environmental Science & Technology*, *50*(8), 4159–4168. https://doi.org/10.1021/acs.est.5b04322

493 Hattori, Y., Suzuki, K., Honda, M., & Shimizu, H. (2003). Re-os isotope systematics of the Taklimakan
494 Desert sands, moraines and river sediments around the taklimakan desert, and of Tibetan soils.
495 *Geochimica et Cosmochimica Acta*, *67*(6), 1195–1205. https://doi.org/10.1016/S0016-
496 7037(00)01206-1

497 Hong, S., Lee, K., Hou, S., Hur, S. Do, Ren, J., Burn, L. J., et al. (2009). An 800-Year Record of
498 Atmospheric As, Mo, Sn, and Sb in Central Asia in High-Altitude Ice Cores from Mt. Qomolangma
499 (Everest), Himalayas. *Environmental Science & Technology*, *43*(21), 8060–8065.
500 https://doi.org/10.1021/es901685u

501 Jacobi, H.-W., Lim, S., Ménégoz, M., Ginot, P., Laj, P., Bonasoni, P., et al. (2015). Black carbon in snow
502 in the upper Himalayan Khumbu Valley, Nepal: observations and modeling of the impact on snow
503 albedo, melting, and radiative forcing. *The Cryosphere*, *9*(4), 1685–1699. https://doi.org/10.5194/tc-
504 9-1685-2015

505 Jeong, C.-H., Wang, J. M., & Evans, G. J. (2016). Source Apportionment of Urban Particulate Matter
506 using Hourly Resolved Trace Metals, Organics, and Inorganic Aerosol Components. *Atmospheric*
507 *Chemistry and Physics Discussions*, 1–32. https://doi.org/10.5194/acp-2016-189

508 Kaspari, S. D., Schwikowski, M., Gysel, M., Flanner, M. G., Kang, S., Hou, S., & Mayewski, P. A.
509 (2011). Recent increase in black carbon concentrations from a Mt. Everest ice core spanning 1860-
510 2000 AD. *Geophysical Research Letters*, *38*(4), n/a-n/a. https://doi.org/10.1029/2010GL046096

511 Kitto, M. E., Anderson, D. L., Gordon, G. E., & Olmez, I. (1992). Rare earth distributions in catalysts and
512 airborne particles. *Environmental Science & Technology*, *26*(7), 1368–1375.
513 https://doi.org/10.1021/es00031a014

514 Krähenbühl, U., Geissbühler, M., Bühler, F., Eberhardt, P., & Finnegan, D. L. (1992). Osmium isotopes
515 in the aerosols of the mantle volcano Mauna Loa. *Earth and Planetary Science Letters*, *110*(1–4),
516 95–98. https://doi.org/10.1016/0012-821X(92)90041-S

517 Lee, K., Hur, S. Do, Hou, S., Burn-Nunes, L. J., Hong, S., Barbante, C., et al. (2011). Isotopic signatures
518 for natural versus anthropogenic Pb in high-altitude Mt. Everest ice cores during the past 800years.
519 *Science of the Total Environment*, *412–413*, 194–202.
520 https://doi.org/10.1016/j.scitotenv.2011.10.002

521 Levasseur, S., Birck, J.-L., & Allègre, C. J. (1999). The osmium riverine flux and the oceanic mass
522 balance of osmium. *Earth and Planetary Science Letters*, *174*(1–2), 7–23.
523 https://doi.org/10.1016/S0012-821X(99)00259-9

524 Li, C., Kang, S., Zhang, Q., & Gao, S. (2012). Geochemical evidence on the source regions of Tibetan
525 Plateau dusts during non-monsoon period in 2008/09. *Atmospheric Environment*, *59*, 382–388.
526 https://doi.org/10.1016/j.atmosenv.2012.06.006

527 Li, C., Bosch, C., Kang, S., Andersson, A., Chen, P., Zhang, Q., et al. (2016). Sources of black carbon to
528 the Himalayan–Tibetan Plateau glaciers. *Nature Communications*, *7*(1), 12574.
529 https://doi.org/10.1038/ncomms12574

Li, D., Ma, B., Jiang, F., & Wang, P. (2011). Nature, genesis and provenance of silt pellets on the ice surface of Glacier No. 1, upper Urumqi River, Tian Shan, Northwestern China. *Quaternary International*, *236*(1–2), 107–115. https://doi.org/10.1016/j.quaint.2010.10.004

Lillis, P. G., & Selby, D. (2013). Evaluation of the rhenium–osmium geochronometer in the Phosphoria petroleum system, Bighorn Basin of Wyoming and Montana, USA. *Geochimica et Cosmochimica Acta*, *118*, 312–330. https://doi.org/10.1016/j.gca.2013.04.021

Łokas, E., Zaborska, A., Kolicka, M., Różycki, M., & Zawierucha, K. (2016). Accumulation of atmospheric radionuclides and heavy metals in cryoconite holes on an Arctic glacier. *Chemosphere*, *160*, 162–172. https://doi.org/10.1016/j.chemosphere.2016.06.051

Love, S. G., & Brownlee, D. E. (1993). A Direct Measurement of the Terrestrial Mass Accretion Rate of Cosmic Dust. *Science*, *262*(5133), 550–553. https://doi.org/10.1126/science.262.5133.550

Maibam, B., Singh, Y. R., Shukla, A. D., & Ramanathan, A. L. (2016). Geochemical Study of the Granitoids Around Chhota Shigri. *Journal of Applied Geochemistry*, *18*(4), 408–413.

Meisel, T., Walker, R. J., Irving, A. J., & Lorand, J.-P. (2001). Osmium isotopic compositions of mantle xenoliths: a global perspective. *Geochimica et Cosmochimica Acta*, *65*(8), 1311–1323. https://doi.org/10.1016/S0016-7037(00)00566-4

Miller, C., Thoni, M., Frank, W., Grasemann, B., Klotzli, U., Guntli, P., & Draganits, E. (2001). The early Palaeozoic magmatic event in the Northwest Himalaya, India: source, tectonic setting and age of emplacement. *Geological Magazine*, *138*(3), 237–251. https://doi.org/10.1017/S0016756801005283

Nagorski, S. A., Kaspari, S. D., Hood, E., Fellman, J. B., & Skiles, S. M. (2019). Radiative Forcing by Dust and Black Carbon on the Juneau Icefield, Alaska. *Journal of Geophysical Research: Atmospheres*, *124*(7), 3943–3959. https://doi.org/10.1029/2018JD029411

Nizam, S., Sen, I. S., Vinoj, V., Galy, V., Selby, D., Azam, M. F., et al. (2020). Biomass-Derived Provenance Dominates Glacial Surface Organic Carbon in the Western Himalaya. *Environmental Science & Technology*, *54*(14), 8612–8621. https://doi.org/10.1021/acs.est.0c02710

Olmez, I., & Gordon, G. E. (1985). Rare Earths: Atmospheric Signatures for Oil-Fired Power Plants and Refineries. *Science*, *229*(4717), 966–968. https://doi.org/10.1126/science.229.4717.966

Owens, P. N., Blake, W. H., & Millward, G. E. (2019). Extreme levels of fallout radionuclides and other contaminants in glacial sediment (cryoconite) and implications for downstream aquatic ecosystems. *Scientific Reports*, *9*(1), 12531. https://doi.org/10.1038/s41598-019-48873-z

Ownsworth, E., Selby, D., Ottley, C. J., Unsworth, E., Raab, A., Feldmann, J., et al. (2019). Tracing the natural and anthropogenic influence on the trace elemental chemistry of estuarine macroalgae and the implications for human consumption. *Science of The Total Environment*, *685*, 259–272. https://doi.org/10.1016/j.scitotenv.2019.05.263

Panwar, S., Agarwal, V., & Chakrapani, G. J. (2017). Morphometric and sediment source characterization of the Alaknanda river basin, headwaters of river Ganga, India. *Natural Hazards*, *87*(3), 1649–1671. https://doi.org/10.1007/s11069-017-2838-y

Parsons, A. J., & Abrahams, A. D. (2009). *Geomorphology of Desert Environments*. (A. J. Parsons & A. D. Abrahams, Eds.), *Geomorphology of Desert Environments*. Dordrecht: Springer Netherlands. https://doi.org/10.1007/978-1-4020-5719-9

Peucker-Ehrenbrink, B., & Blum, J. D. (1998). Re-Os isotope systematics and weathering of Precambrian crustal rocks: implications for the marine osmium isotope record. *Geochimica et Cosmochimica Acta*, *62*(19–20), 3193–3203. https://doi.org/10.1016/S0016-7037(98)00227-0

574 Peucker-Ehrenbrink, B., & Jahn, B. (2001). Rhenium-osmium isotope systematics and platinum group
575 element concentrations: Loess and the upper continental crust. *Geochemistry, Geophysics,*
576 *Geosystems*, *2*(10), 2001GC000172. https://doi.org/10.1029/2001GC000172

577 Pierson-Wickmann, A.-C., Reisberg, L., & France-Lanord, C. (2000). The Os isotopic composition of
578 Himalayan river bedloads and bedrocks: importance of black shales. *Earth and Planetary Science*
579 *Letters*, *176*(2), 203–218. https://doi.org/10.1016/S0012-821X(00)00003-0

580 Poirier, A., & Gariépy, C. (2005). Isotopic Signature and Impact of Car Catalysts on the Anthropogenic
581 Osmium Budget. *Environmental Science & Technology*, *39*(12), 4431–4434.
582 https://doi.org/10.1021/es0484552

583 Prasad, A. K., Yang, K.-H. S., El-Askary, H. M., & Kafatos, M. (2009). Melting of major Glaciers in the
584 western Himalayas: evidence of climatic changes from long term MSU derived tropospheric
585 temperature trend (1979–2008). *Annales Geophysicae*, *27*(12), 4505–4519.
586 https://doi.org/10.5194/angeo-27-4505-2009

587 Pye, K. (1995). The nature, origin and accumulation of loess. *Quaternary Science Reviews*, *14*(7–8), 653–
588 667. https://doi.org/10.1016/0277-3791(95)00047-X

589 Ramsankaran, R., Pandit, A., & Azam, M. F. (2018). Spatially distributed ice-thickness modelling for
590 Chhota Shigri Glacier in western Himalayas, India. *International Journal of Remote Sensing*,
591 *39*(10), 3320–3343. https://doi.org/10.1080/01431161.2018.1441563

592 Ran, L., Lin, W. L., Deji, Y. Z., La, B., Tsering, P. M., Xu, X. B., & Wang, W. (2014). Surface gas
593 pollutants in Lhasa, a highland city of Tibet – current levels and pollution implications. *Atmospheric*
594 *Chemistry and Physics*, *14*(19), 10721–10730. https://doi.org/10.5194/acp-14-10721-2014

595 Ranjan, N., & Banerjee, D. M. (2009). Central Himalayan crystallines as the primary source for the
596 sandstone–mudstone suites of the Siwalik Group: New geochemical evidence. *Gondwana Research*,
597 *16*(3–4), 687–696. https://doi.org/10.1016/j.gr.2009.07.005

598 Rauch, S., Hemond, H. F., Peucker-Ehrenbrink, B., Ek, K. H., & Morrison, G. M. (2005). Platinum
599 Group Element Concentrations and Osmium Isotopic Composition in Urban Airborne Particles from
600 Boston, Massachusetts. *Environmental Science & Technology*, *39*(24), 9464–9470.
601 https://doi.org/10.1021/es051310q

602 Rodushkin, I., Engström, E., Sörlin, D., Pontér, C., & Baxter, D. C. (2007). Osmium in environmental
603 samples from Northeast Sweden. Part II. Identification of anthropogenic sources. *Science of The*
604 *Total Environment*, *386*(1–3), 159–168. https://doi.org/10.1016/j.scitotenv.2007.06.012

605 Roy, P. D., & Smykatz-Kloss, W. (2007). REE geochemistry of the recent playa sediments from the Thar
606 Desert, India: An implication to playa sediment provenance. *Geochemistry*, *67*(1), 55–68.
607 https://doi.org/10.1016/j.chemer.2005.01.006

608 Rudnick, R. L., & Gao, S. (2014). Composition of the Continental Crust. In K. K. T. Heinrich D. Holland
609 (Ed.), *Treatise on Geochemistry* (2nd ed., Vol. 4, pp. 1–51). Elsevier. https://doi.org/10.1016/B978-
610 0-08-095975-7.00301-6

611 Rupakheti, D., Adhikary, B., Praveen, P. S., Rupakheti, M., Kang, S., Mahata, K. S., et al. (2017). Pre-
612 monsoon air quality over Lumbini, a world heritage site along the Himalayan foothills. *Atmospheric*
613 *Chemistry and Physics*, *17*(18), 11041–11063. https://doi.org/10.5194/acp-17-11041-2017

614 Rupakheti, D., Kang, S., Rupakheti, M., Tripathee, L., Zhang, Q., Chen, P., & Yin, X. (2018). Long-term
615 trends in the total columns of ozone and its precursor gases derived from satellite measurements
616 during 2004–2015 over three different regions in South Asia: Indo-Gangetic Plain, Himalayas and
617 Tibetan Plateau. *International Journal of Remote Sensing*, *39*(21), 7384–7404.
618 https://doi.org/10.1080/01431161.2018.1470699

Saikawa, E., Panday, A., Kang, S., Gautam, R., Zusman, E., Cong, Z., et al. (2019). *The Hindu Kush Himalaya Assessment*. (P. Wester, A. Mishra, A. Mukherji, & A. B. Shrestha, Eds.), *The Hindu Kush Himalaya Assessment*. Cham: Springer International Publishing. https://doi.org/10.1007/978-3-319-92288-1

Schmitz, B., Peucker-Ehrenbrink, B., Lindström, M., & Tassinari, M. (1997). Accretion Rates of Meteorites and Cosmic Dust in the Early Ordovician. *Science*, *278*(5335), 88–90. https://doi.org/10.1126/science.278.5335.88

Selby, D., & Creaser, R. A. (2003). Re–Os geochronology of organic rich sediments: an evaluation of organic matter analysis methods. *Chemical Geology*, *200*(3–4), 225–240. https://doi.org/10.1016/S0009-2541(03)00199-2

Selby, D., Creaser, R. A., & Fowler, M. G. (2007). Re–Os elemental and isotopic systematics in crude oils. *Geochimica et Cosmochimica Acta*, *71*(2), 378–386. https://doi.org/10.1016/j.gca.2006.09.005

Selby, D., Mutterlose, J., & Condon, D. J. (2009). U–Pb and Re–Os geochronology of the Aptian/Albian and Cenomanian/Turonian stage boundaries: Implications for timescale calibration, osmium isotope seawater composition and Re–Os systematics in organic-rich sediments. *Chemical Geology*, *265*(3–4), 394–409. https://doi.org/10.1016/j.chemgeo.2009.05.005

Sen, I. S., Peucker-Ehrenbrink, B., & Geboy, N. (2013). Complex Anthropogenic Sources of Platinum Group Elements in Aerosols on Cape Cod, USA. *Environmental Science & Technology*, *47*(18), 130827135610007. https://doi.org/10.1021/es4016348

Sen, I. S., Bizimis, M., Tripathi, S. N., & Paul, D. (2016). Lead isotopic fingerprinting of aerosols to characterize the sources of atmospheric lead in an industrial city of India. *Atmospheric Environment*, *129*, 27–33. https://doi.org/10.1016/j.atmosenv.2016.01.005

Shao, Y. (2009). *Physics and Modelling of Wind Erosion*. (Y. Shao, Ed.), *Springer-Verlag, Berlin Heidelberg* (Vol. 37). Dordrecht: Springer Netherlands. https://doi.org/10.1007/978-1-4020-8895-7

Sharp, M., Tranter, M., Brown, G. H., & Skidmore, M. (1995). Rates of chemical denudation and CO drawdown in a glacier-covered alpine catchment. *Geology*, *23*(1), 61. https://doi.org/10.1130/0091-7613(1995)023<0061:ROCDAC>2.3.CO;2

Shrestha, P., Barros, A. P., & Khlystov, A. (2010). Chemical composition and aerosol size distribution of the middle mountain range in the Nepal Himalayas during the 2009 pre-monsoon season. *Atmospheric Chemistry and Physics*, *10*(23), 11605–11621. https://doi.org/10.5194/acp-10-11605-2010

Singh, P., Sarawade, P., & Adhikary, B. (2020). Transport of black carbon from planetary boundary layer to free troposphere during the summer monsoon over South Asia. *Atmospheric Research*, *235*, 104761. https://doi.org/10.1016/j.atmosres.2019.104761

Singh, S. K., Trivedi, J. R., & Krishnaswami, S. (1999). Re-Os isotope systematics in black shales from the Lesser Himalaya: their chronology and role in the 187Os/188Os evolution of seawater. *Geochimica et Cosmochimica Acta*, *63*(16), 2381–2392. https://doi.org/10.1016/S0016-7037(99)00201-X

Singh, S. M., Sharma, J., Gawas-Sakhalkar, P., Upadhyay, A. K., Naik, S., Pedneker, S. M., & Ravindra, R. (2013). Atmospheric deposition studies of heavy metals in Arctic by comparative analysis of lichens and cryoconite. *Environmental Monitoring and Assessment*, *185*(2), 1367–1376. https://doi.org/10.1007/s10661-012-2638-5

Sproson, A. D., Selby, D., Suzuki, K., Oda, T., & Kuroda, J. (2020). Anthropogenic Osmium in Macroalgae from Tokyo Bay Reveals Widespread Contamination from Municipal Solid Waste. *Environmental Science & Technology*, *54*(15), 9356–9365. https://doi.org/10.1021/acs.est.0c01602

Srivastava, R. K., & Samal, A. K. (2019). Geochemical characterization, petrogenesis, and emplacement tectonics of Paleoproterozoic high-Ti and low-Ti mafic intrusive rocks from the western Arunachal Himalaya, northeastern India and their possible relation to the ~1.9 Ga LIP event of the Indian s. *Geological Journal*, *54*(1), 245–265. https://doi.org/10.1002/gj.3172

Stockwell, C. E., Christian, T. J., Goetz, J. D., Jayarathne, T., Bhave, P. V., Praveen, P. S., et al. (2016). Nepal Ambient Monitoring and Source Testing Experiment (NAMaSTE): emissions of trace gases and light-absorbing carbon from wood and dung cooking fires, garbage and crop residue burning, brick kilns, and other sources. *Atmospheric Chemistry and Physics*, *16*(17), 11043–11081. https://doi.org/10.5194/acp-16-11043-2016

Taylor, S. R., & McLennan, S. M. (1985). *The continental crust: Its composition and evolution*. States, United: Blackwell, Oxford.

Thakur, S. S., & Patel, S. C. (2012). Mafic and pelitic xenoliths in the Kinnaur Kailash Granite, Baspa river valley, NW Himalaya: Evidence of pre-Himalayan granulite metamorphism followed by cooling event. *Journal of Asian Earth Sciences*, *56*, 105–117. https://doi.org/10.1016/j.jseaes.2012.04.024

Thöni, M., Miller, C., Hager, C., Grasemann, B., & Horschinegg, M. (2012). New geochronological constraints on the thermal and exhumation history of the Lesser and Higher Himalayan Crystalline Units in the Kullu–Kinnaur area of Himachal Pradesh (India). *Journal of Asian Earth Sciences*, *52*, 98–116. https://doi.org/10.1016/j.jseaes.2012.02.015

Thorpe, M. T., Hurowitz, J. A., & Dehouck, E. (2019). Sediment geochemistry and mineralogy from a glacial terrain river system in southwest Iceland. *Geochimica et Cosmochimica Acta*, *263*, 140–166. https://doi.org/10.1016/j.gca.2019.08.003

Tranter, M., Sharp, M. J., Lamb, H. R., Brown, G. H., Hubbard, B. P., & Willis, I. C. (2002). Geochemical weathering at the bed of Haut Glacier d'Arolla, Switzerland?a new model. *Hydrological Processes*, *16*(5), 959–993. https://doi.org/10.1002/hyp.309

Vincent, C., Ramanathan, A., Wagnon, P., Dobhal, D. P., Linda, A., Berthier, E., et al. (2013). Balanced conditions or slight mass gain of glaciers in the Lahaul and Spiti region (northern India, Himalaya) during the nineties preceded recent mass loss. *The Cryosphere*, *7*(2), 569–582. https://doi.org/10.5194/tc-7-569-2013

Wagnon, P., Linda, A., Arnaud, Y., Kumar, R., Sharma, P., Vincent, C., et al. (2007). Four years of mass balance on Chhota Shigri Glacier, Himachal Pradesh, India, a new benchmark glacier in the western Himalaya. *Journal of Glaciology*, *53*(183), 603–611. https://doi.org/10.3189/002214307784409306

Wake, C. P., Mayewski, P. A., Zichu, X., Ping, W., & Zhongqin, L. (1993). Regional distribution of monsoon and desert dust signals recorded in Asian glaciers. *Geophysical Research Letters*, *20*(14), 1411–1414. https://doi.org/10.1029/93GL01682

Walker, R. ., Horan, M. ., Morgan, J. ., Becker, H., Grossman, J. ., & Rubin, A. . (2002). Comparative 187Re-187Os systematics of chondrites. *Geochimica et Cosmochimica Acta*, *66*(23), 4187–4201. https://doi.org/10.1016/S0016-7037(02)01003-7

Xu, B., Cao, J., Hansen, J., Yao, T., Joswia, D. R., Wang, N., et al. (2009). Black soot and the survival of Tibetan glaciers. *Proceedings of the National Academy of Sciences*, *106*(52), 22114–22118. https://doi.org/10.1073/pnas.0910444106

Yan, F., He, C., Kang, S., Chen, P., Hu, Z., Han, X., et al. (2019). Deposition of Organic and Black Carbon: Direct Measurements at Three Remote Stations in the Himalayas and Tibetan Plateau. *Journal of Geophysical Research: Atmospheres*, *124*(16), 9702–9715. https://doi.org/10.1029/2019JD031018

Yang, X., Lu, D., Tan, J., Sun, X., Zhang, Q., Zhang, L., et al. (2020). Two-Dimensional Silicon Fingerprints Reveal Dramatic Variations in the Sources of Particulate Matter in Beijing during 2013–2017. *Environmental Science & Technology*, *54*(12), 7126–7135. https://doi.org/10.1021/acs.est.0c00984

Yarragunta, Y., Srivastava, S., Mitra, D., & Chandola, H. C. (2020). Influence of forest fire episodes on the distribution of gaseous air pollutants over Uttarakhand, India. *GIScience & Remote Sensing*, *57*(2), 190–206. https://doi.org/10.1080/15481603.2020.1712100

Yudovskaya, M. A., Tessalina, S., Distler, V. V., Chaplygin, I. V., Chugaev, A. V., & Dikov, Y. P. (2008). Behavior of highly-siderophile elements during magma degassing: A case study at the Kudryavy volcano. *Chemical Geology*, *248*(3–4), 318–341. https://doi.org/10.1016/j.chemgeo.2007.12.008

Zhang, Q., Kang, S., Kaspari, S., Li, C., Qin, D., Mayewski, P. A., & Hou, S. (2009). Rare earth elements in an ice core from Mt. Everest: Seasonal variations and potential sources. *Atmospheric Research*, *94*(2), 300–312. https://doi.org/10.1016/j.atmosres.2009.06.005

724

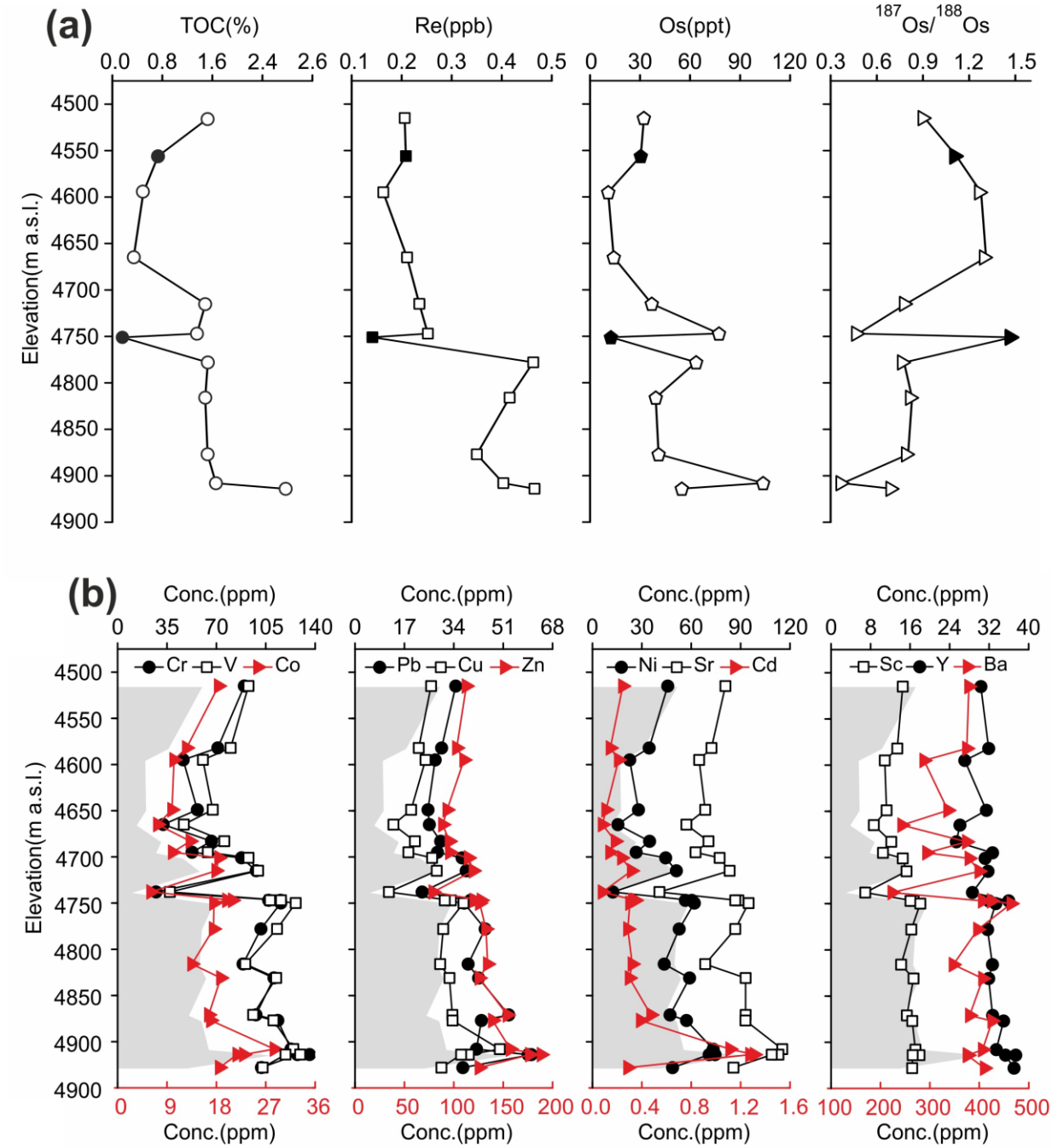

725

726 **Figure 1.** (a) Rhenium-Osmium concentration, $^{187}Os/^{188}Os$ ratios and Total Organic Carbon (TOC)
727 in cryoconite (open symbols) and fine moraine fraction (<63µm, filled symbols) (b) Trace metal
728 concentration in cryoconite and TOC (scale is identical to a) along the ablation zone of the CSG.
729 TOC data are from (Nizam et al., 2020)

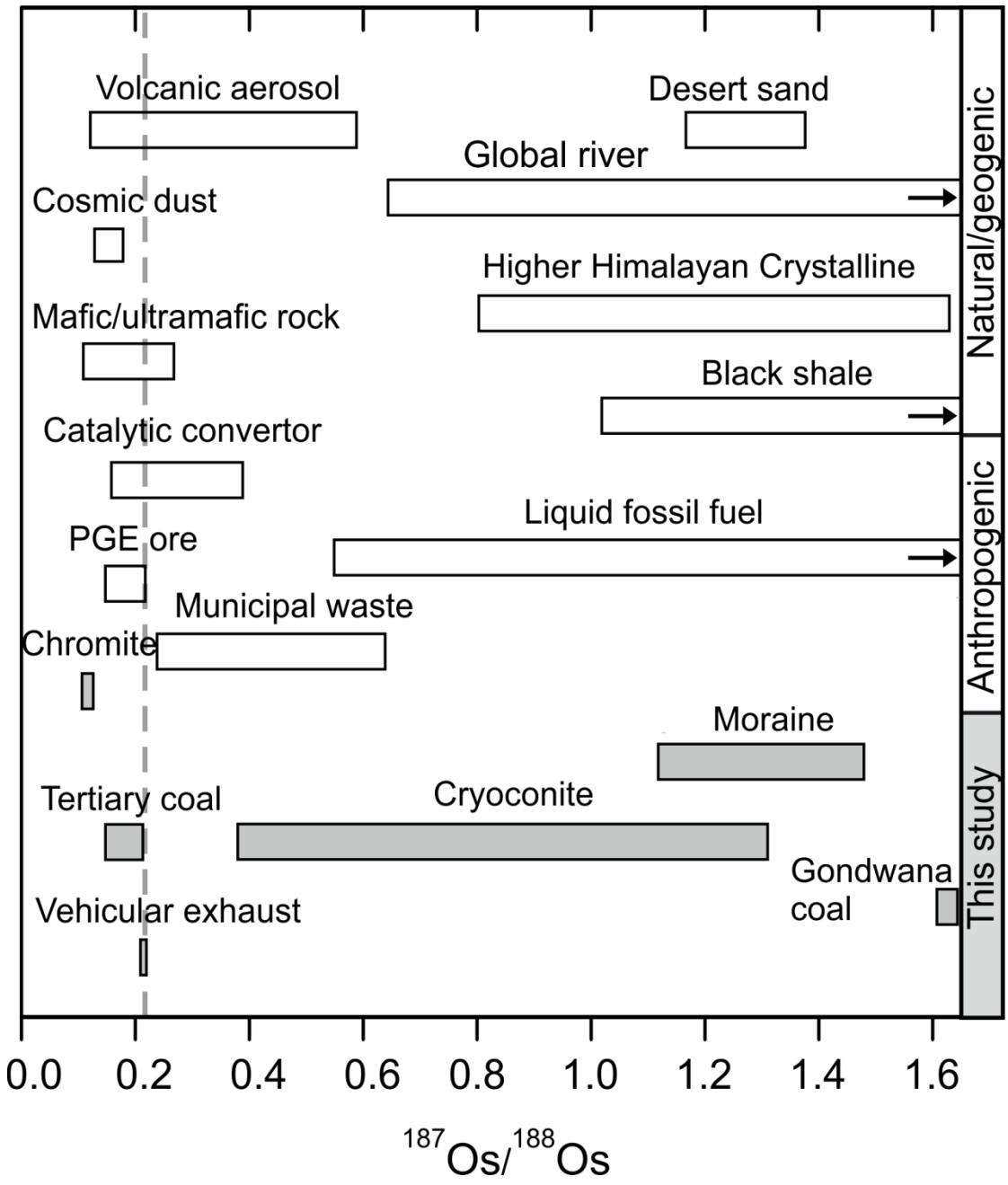

Figure 2. Comparison of osmium isotopic ratio of cryoconite and moraine with different potential sources. The dashed vertical line marks the limit of the measured unradiogenic Os that can be directly contributed by vehicular emission in the atmosphere. Moraine Os isotopic ratios lie within the crustal range of both eroding i.e. global river (Levasseur et al., 1999) and non-eroding crust: Higher Himalayan Crystalline Sequence (Pierson-Wickmann et al., 2000), black shale (van Acken et al., 2019; Ackerman et al., 2019; Selby & Creaser, 2003; S. K. Singh et al., 1999). Cryoconite, in contrast, exhibits a range in $^{187}Os/^{188}Os$ ratios that encompass a crustal signature to an

738 unradiogenic signature similar to that of recycled catalytic converters (Poirier & Gariépy, 2005),
739 volcanic aerosol (Krähenbühl et al., 1992; Yudovskaya et al., 2008) and municipal waste (Funari
740 et al., 2016). Data reference: cosmic dust (Schmitz et al., 1997; Walker et al., 2002),
741 mafic/ultramafic rock (Hanski et al., 2001; Meisel et al., 2001), Taklimakan desert and Kunlun
742 moraine (Hattori et al., 2003), catalytic convertor (Poirier and Gariépy, 2005), liquid fossil fuel
743 (Corrick et al., 2019; Cumming et al., 2014; Lillis & Selby, 2013; Selby et al., 2007), chromite ore
744 (Mondal et al., 2007), PGE ore (Coggon et al., 2012), and municipal waste (Funari et al., 2016).

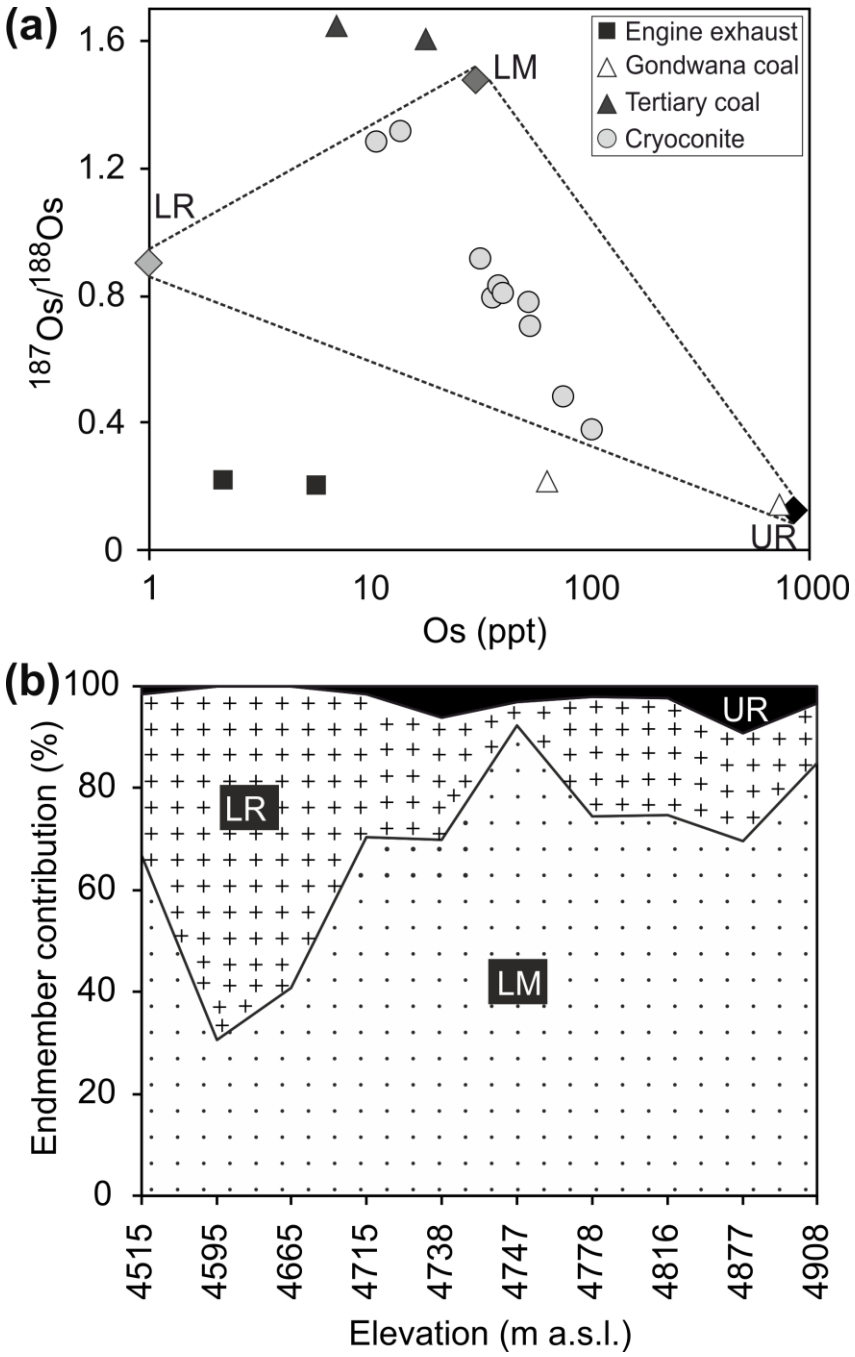

Figure 3. (a) Three-component mixing modeling plot for Os concentration and $^{187}Os/^{188}Os$ for cryoconite and the proposed three end-members: LM (Local Moraine), LR (Less Radiogenic Os poor mineral phase: aeolian quartz/granite/orthogneiss), and UR (Ultramafic Rocks). (b) Source percent contribution of the Os within the collected cryoconite relative to elevation along the ablation zone of the CSG. See text for discussion.

752 **Table 1.** Re-Os isotopes composition and Re-Os abundance analyzed in selected cryoconite (C), moraine
753 (DF:<63 μm), diesel engine exhaust (DEE) and Indian coal (GC: Gondwana coal, TC: Tertiary coal)
754 samples.

Sample	Total Re (2s) ($ng\ g^{-1}$)	Total Os (2s) ($pg\ g^{-1}$)	^{192}Os (2s) ($pg\ g^{-1}$)	$^{187}Re/^{188}Os$ 2s	$^{187}Os/^{188}Os$ 2s	rho	%Re Blank	$\%^{187}Os$ Blank	$\%^{188}Os$ Blank
C1	0.206± 0.002	32.3± 0.2	12.1± 0.1	33.8± 0.4	0.911± 0.008	0.402	1.16	0.09	0.33
C3	0.163± 0.002	10.9± 0.1	3.9± 0.1	83± 1.4	1.278± 0.170	0.599	1.47	0.2	1.03
C5	0.211± 0.002	14.2± 0.1	5.1± 0.1	82.4± 1.1	1.310± 0.015	0.596	1.13	0.15	0.79
C9	0.235± 0.002	37± 0.2	14.1± 0.1	33.3± 0.4	0.790± 0.007	0.414	1.02	0.09	0.29
C11	0.252± 0.002	77.3± 0.3	30.5± 0.2	16.4± 0.2	0.479± 0.004	0.386	0.95	0.07	0.13
C13	0.463± 0.002	63.6± 0.3	24.2± 0.1	38.1± 0.3	0.777± 0.006	0.522	0.52	0.05	0.17
C14	0.416± 0.002	39.4± 0.2	14.9± 0.1	55.5± 0.5	0.829± 0.007	0.543	0.58	0.08	0.27
C17	0.35± 0.002	41.1± 0.2	15.6± 0.1	44.7± 0.4	0.803± 0.006	0.504	0.69	0.08	0.26
C18	0.403± 0.002	104± 0.4	41.5± 0.2	19.3± 0.2	0.378± 0.003	0.483	0.6	0.06	0.1
C19	0.465± 0.002	55± 0.2	21.1± 0.1	43.9± 0.3	0.702± 0.006	0.531	0.51	0.07	0.19
DF6	0.208± 0.002	30.4± 0.2	11.1± 0.1	37.4± 0.5	1.118± 0.010	0.408	1.15	0.08	0.36
DF12	0.141± 0.002	12.5± 0.1	4.4± 0.1	63.9± 1.2	1.478± 0.018	0.518	1.7	0.15	0.91
GC1	0.261± 0.002	6.9± 0.1	2.4± 0.1	217± 8.2	1.644± 0.069	0.856	4.39	0.83	6.38
GC2	0.757± 0.003	17.9± 0.1	6.2± 0.1	243± 4.2	1.606± 0.032	0.801	1.52	0.33	2.56
TC1	0.527± 0.003	726± 2.8	299± 2.6	3.5± 0.04	0.144± 0.002	0.609	2.18	0.08	0.05
TC2	0.468± 0.002	63.4± 0.3	25.9± 0.3	35.9± 0.4	0.213± 0.003	0.562	2.46	0.59	0.63
DEE1	0.073± 0.011	2.1± 0.5	0.9± 0.5	166± 95	0.218± 0.185	0.631	48.4	63.23	40.75
DEE2	1.032± 0.018	5.7± 0.8	2.3± 0.8	884± 294	0.205± 0.126	0.541	10.48	64.54	39.86

755 Note: Total procedural blanks were 2.1 ppt for Re and 0.1 ppt for Os, with a $^{187}Os/^{188}Os$ ratio of 0.25.